Eur. Phys. J. AP **22**, 41–49 (2003)
DOI: 10.1051/epjap:2003006

THE EUROPEAN PHYSICAL JOURNAL
APPLIED PHYSICS

Electric wind characterisation in negative point-to-plane corona discharges in air

Ph. Béquin[a], K. Castor, and J. Scholten

Laboratoire d'Acoustique de l'Université du Maine, UMR – CNRS 6613, Université du Maine, avenue Olivier Messiaen, 72085 Le Mans Cedex 9, France

Received: 4 January 2002 / Received in final form: 28 October 2002 / Accepted: 10 December 2002
Published online: 25 February 2003 –

Abstract. In point-to-plane corona discharges in air, the collisions of charged particles with neutral particles induce a gas movement between the point to the plane called electric wind. A one-dimensional model of the neutral particle velocity along the discharge axis and between the electrodes is first developed. Laser Doppler Anemometry is used to measure the axial velocity profile of the gas between the electrodes. Discrepancies between experimental results and predictions of the on-axis velocity are discussed. Finally, the measured velocity profile compares quite well with a $\cos^5\theta$ distribution. Significant differences between measured and $\cos^5\theta$ profiles are observed near the discharge axis which could be attributed to the presence of seeding particles.

PACS. 51.10.+y Kinetic and transport theory of gases – 51.35.+a Mechanical properties; compressibility – 52.80.Hc Glow; corona

1 Introduction

Various aspects of corona discharges in atmospheric air have been extensively studied both experimentally and theoretically [1–8]. However, the gas flow between point-to-plane electrodes has not yet been investigated in detail. This is largely due to the difficulty in measuring the particle velocity without disturbing the electric and geometric properties of the corona discharges.

The objective of this work is to measure the particle velocity distribution in negative point-to-plane corona in air with normal atmospheric conditions by means of Laser Doppler Anemometry (LDA), and to compare the measurements with predictions. The first section of the paper deals with the properties of the point-to-plane corona discharges. The next section introduces a one-dimensional model of the neutral particle velocity which is based on a work first presented by Robinson [9] and Sigmond *et al.* [10–12]. The third section presents the LDA technique and the measured on-axis velocities of the gas flow between the electrodes. In the fourth section, the gas velocity profiles (off-axis velocity) are measured and discussed. The final section gives conclusions and makes recommendations for further work.

[a] e-mail: philippe.bequin@univ-lemans.fr

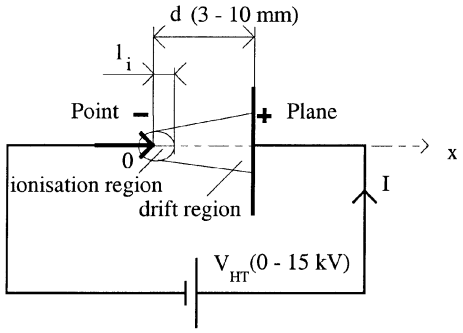

Fig. 1. Point-to-plane system. V_{HT}, I, d, and l_{i} represent respectively the supplied voltage, the electric current, the gap length and the length of the ionisation region.

2 Negative point-to-plane corona discharges

Corona discharges are produced in a non-uniform electric field which can be provided by a variety of electrode configurations and shapes. A convenient and often used one is the point-to-plane electrode configuration. When a high DC negative voltage V_{HT} is applied to the point of a point-to-plane system, air in the vicinity of the electrode with a small radius of curvature becomes ionised (Fig. 1). The charged particles so created form a cloud drifting along the field lines. Because of the geometric effect and the local presence of the cloud, the electric field between electrodes is strongly nonuniform and varies with time as successive clouds drift from one electrode to the other. This

phenomenon gives a pulsating electric current in the external circuit [3,8,13–15] and causes an electric wind flowing from the point toward the plane [9–12,16–18].

Considering a time-averaged distribution of the electric field between the electrodes during a single pulse [19], two regions can be distinguished (Fig. 1). The first one, termed the ionisation region, is located at the tip of the point and is characterised by a value of the field higher than the "critical" value E_c ($E_c \approx 27$ kV/cm in air) of the electric field for which electron production by ionisation is exactly compensated by attachment of the electrons on neutral particles. In this region the presence of a sufficiently strong electric field makes the ionisation processes predominant. The field accelerates the free charged particles to undergo ionising collisions with air molecules in the gap generating more electrons and positive ions. During the discharge, the positive ions flow toward the point and induce a ring vortex close to the point. This last phenomena has been pointed out theoretically and numerically by Sigmond *et al.* [11,12].

The second region, termed the drift region, takes place between the ionisation region and the plane, and is characterised by a weaker and an almost uniform value of the electric field ($E \ll E_c$). Electrons produced by ionisation drift along the weak electric field: the more energetic ones reach the collecting plane, whereas the less energetic ones are captured by neutral particles and then become negative ions (attachment processes predominant). The collisions of charged particles with neutral particle induces movement of air known as electric wind or ionic wind.

3 Electric wind model – on-axis axial velocity

A literature review dealing with the electric wind is given by Owsenek *et al.* [20] and Sigmond and Lågstad [12]. Robinson [9] and more recently Sigmond *et al.* [10–12] derived an equation modelling one-dimensional electric wind velocity outside the gap and showed that the velocity is proportional to the square root of the discharge current. The model described here is a development of this earlier finding. In the following sections Robinson's work has been the underlying basis, but the fundamentals are expanded to clarify the method, and the results are extended to include, among other details, the fitted parameter $\beta = I_e/I_i$ (the ratio of the electric currents I_i and I_e carried by the electrons and the ions). Very recently Batina *et al.* [21] has investigated electric wind in a closed vessel with a positive point-to-plane device. The theoretical and numerical results obtained by Batina *et al.* [21] cannot be directly used or compared with the results of the present study because of the different behaviour between positive and negative discharges and significant differences between flows in a confined enclosure (closed vessel) as opposed to an infinite environment (because of the recirculating flow).

This study deals with the hydrodynamic behaviour of the neutral particles in the drift region (Fig. 1). The gas is assumed to be weakly ionised: the density of charged particles is assumed to be much less than the density of neutral particles. A term-by-term analysis of the equations for charged particles in a weakly ionised gas shows the balance between the electric field providing a source of energy and the loss of energy through both elastic and inelastic particle collisions [22–27].

The equation of momentum conservation for neutral particles can be written as:

$$\rho \frac{\mathrm{d}\mathbf{V}_g}{\mathrm{d}t} = -\boldsymbol{\nabla} P + \boldsymbol{\nabla} \cdot \left[\bar{\bar{\tau}}\right] + \mathbf{F} \quad \text{with } \frac{\mathrm{d}}{\mathrm{d}t} = \frac{\partial}{\partial t} + \mathbf{V}_g \cdot \mathbf{grad}, \tag{1}$$

where ρ, P and $\mathbf{V}_g$ are respectively the neutral-gas particle density, the pressure and the macroscopic gas velocity. The viscous stress tensor $\left[\bar{\bar{\tau}}\right]$ accounts for the viscosity phenomena which are associated with the collisions between neutral particles. The quantity $\mathbf{F}$, having a dimension of force per unit volume, is similar to an external action for the gas (predominantly composed of neutral particles), although it is associated with the internal collisions between charged and neutral particles. The associated macroscopic effect is important only in the drift region, where all charged particles flow roughly along the almost parallel field lines.

The momentum of the charged particles is drawn from the total electric field and is transferred to the neutral-gas particles through collisions, the quantity $\mathbf{F}$ is given by

$$\mathbf{F} \approx \sum_i N_i \left(\frac{m_i}{m}\right) q\mathbf{E}, \tag{2}$$

where $\mathbf{E}$ is the total electric field; m and m_i represent the neutral particle mass and the charged particle mass, respectively. The quantity N_i is the charged particle density. The quantity $\mathbf{F}$ becomes important for either N_i high or for a mass ratio (m_i/m) close to unity, and then is predominantly related to collisions between negative ions and neutral particles.

In order to find an approximate analytical solution of equation (1), the following assumptions are used:

- a steady flow is assumed ($\frac{\partial}{\partial t} \equiv 0$);
- a parallel flow is considered, all fluid particles move in the same direction (axis of the point);
- the static pressure is assumed to be constant in the whole gap: $\nabla P = 0$;
- the viscosity effects are ignored;
- the electron action on the neutral particles is negligible compared to the negative ion action and the ratio (m_i/m) is considered close to unity:

$$\mathbf{F} \approx N_i \left(\frac{m_i}{m}\right) q\mathbf{E} \approx N_i q\mathbf{E}. \tag{3}$$

Using the relation between the current density associated to the negative ion $\mathbf{J}_i$ and the total electric field

$$\mathbf{J}_i = N_i q \mu_i \mathbf{E}, \tag{4}$$

with the above assumptions, the equation of momentum conservation for neutral particles is reduced to

$$V_g \cdot \frac{\partial V_g}{\partial x} = +\frac{J_i}{\rho \mu_i}, \tag{5}$$

where μ_i is the mobility of the negative ions ($\mu_\mathrm{i} \approx 1.8 \times 10^{-4}$ [V m^2 s^{-1}]) and J_i is the on-axis current density assumed to be roughly constant between the electrodes. The solution of this ordinary differential equation is deduced to be

$$V_\mathrm{g}^2(x) = \frac{2J_\mathrm{i}}{\rho\mu_\mathrm{i}}(x - l_\mathrm{i}) + V_{x=l_\mathrm{i}}^2, \tag{6}$$

where x is the on-axis location between the electrodes, l_i the length of the ionisation region, and $V_{x=l_\mathrm{i}}$ the velocity on the interface between the ionisation and the drift region (Fig. 1).

The current density J_i is now substituted by the total electric current I which can be directly measured. Using the relation

$$I = I_\mathrm{i} + I_\mathrm{e} = I_\mathrm{i}\left(1 + \frac{I_\mathrm{e}}{I_\mathrm{i}}\right) = I_\mathrm{i}(1 + \beta), \tag{7}$$

where $\beta = \frac{I_\mathrm{e}}{I_\mathrm{i}}$ is the ratio of the electric currents I_e and I_i carried by the electrons and the ions.

With the empirical formula between the current density and the current carried by the negative ions (Warburg law) [28–30]

$$I_\mathrm{i} = \frac{2\pi d^2}{m-2}\left[1 - \cos^{(m-2)}\theta\right] J_\mathrm{i}(r=0)$$

with $m \approx 5$ for negative discharges; finally

$$I_\mathrm{i} \approx \frac{2\pi}{3} d^2 J_\mathrm{i}(r=0). \tag{8}$$

The gas velocity in the drift region can be expressed as:

$$V_\mathrm{g}(x) = \sqrt{\frac{I}{\rho\mu_\mathrm{i}}\frac{3}{\pi d^2}\frac{1}{(1+\beta)}(x - l_\mathrm{i}) + V_{x=l_\mathrm{i}}^2}. \tag{9}$$

The gas velocity is proportional to the square root of the discharge current I, which is in accordance with Robinson [9], and is a function of the square root of the location $(x - l_\mathrm{i})$ from the ionisation region.

4 Experimental set-up and results

The main objective of this section is to measure the on-axis gas velocity in a point-to-plane corona discharge by means of Laser Doppler Anemometer. To the best of our knowledge, due to the complexity of the technique, very few studies have been carried out concerning this measure [17,31,32].

4.1 Experimental set-up

The point-to-plane system is made up of a stainless steel needle connected with a 1 MΩ current limiting resistance (Fig. 2). The needle axis is placed perpendicular to a circular flat steel wire gauze (mesh 0.05×0.05 mm^2; $\varnothing_\mathrm{wire} = 0.03$ mm). Most of the measurements have been made using one needle having a point radius curvature equal to 45 μm. The frame allows the needle-to-grid gap to be varied from 3 to 10 mm. This frame has been rigidly fixed over a metallic plate. This plate is the cover of a box containing all required electronics, which are thus wired in a fixed position relative to the electrodes.

Inside the box, the system described previously is connected in series with a resistance R_1. The set is fed from an adjustable DC power supply (V_HT) in order to generate corona discharges between electrodes. The supply voltage values V_HT are in the range 3 to 8 kV with an associated DC current value I in the range of 25 to 80 μA. The total current I that flows through the air gap is estimated by the measure of the voltage V_I across the resistance R_1, and a high-voltage probe allows to measure the voltage V_HT to be measured across the electrodes. All measurements have been performed in ambient air at atmospheric pressure. The set-up was calibrated in order to remove the influence of all electronic circuits but also to estimate parasitic impedance [19,33].

4.2 Laser Doppler anemometry

For measurement of local flow velocity, the Laser Doppler Anemometer (LDA) is in competition with Pitot Tubes and hot-wire anemometers. Its main advantages relative to these more well-established technique include:

- measurement of velocity is direct rather than by inference from pressure (Pitot tube) or heat-transfer coefficient with non-linear characteristics (hot-wire);
- probe volume can be small (≈0.05 mm^3).

However, LDA has two main drawbacks:

- the necessity for seeding particles in the fluid;
- the complexity of the apparatus, which requires a substantial know-how for an efficient use.

The basic principle of LDA in fluid is described in Figure 3 [34]. A beam splitter divides a laser beam into two coherent beams. Beam optics cause these beams to cross and focus in order to generate an ellipsoidal measuring volume, in which the electromagnetic interferences lead to apparent dark and bright fringes. A seeding particle passing through the probe volume scatters the light from both beams, leading to a diffused light which is detected by a photomultiplier. The electronic signal obtained, called a burst, is weighted by the Gaussian light intensity distribution across the beams section, and frequency modulated by the presence of the interference fringes. The resulting modulation frequency, usually called Doppler frequency f_d, is given by the ratio of the velocity component V_parX normal to the fringes on the fringe spacing e (≈1 μm):

$$f_\mathrm{d} = \frac{V_\mathrm{parX}}{e} = \frac{\sin(\theta/2)}{\lambda/2} V_\mathrm{parX} \tag{10}$$

where λ (≈514.5 nm) is the laser wavelength and θ (≈30°) the beams angle (Fig. 3).

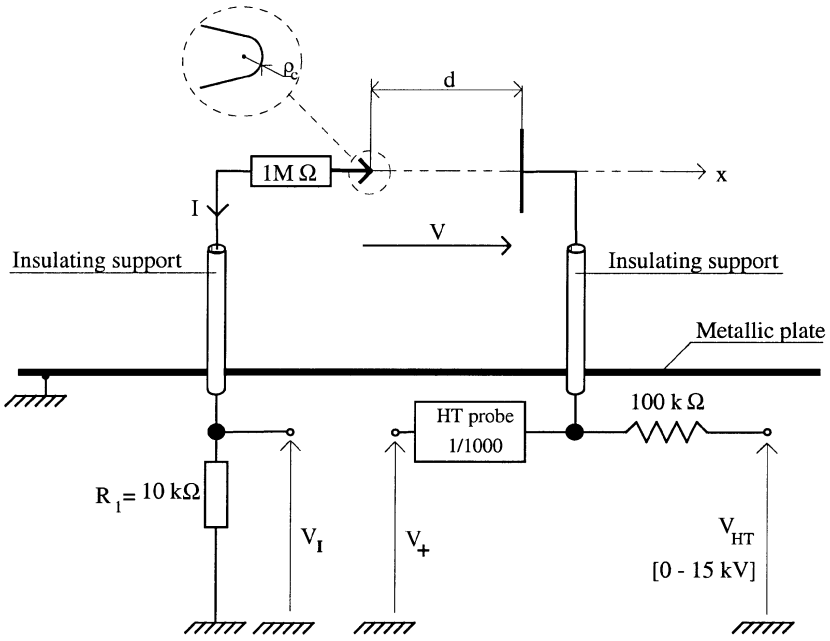

Fig. 2. Schematic representation of the experimental set-up used to measure the electric parameters.

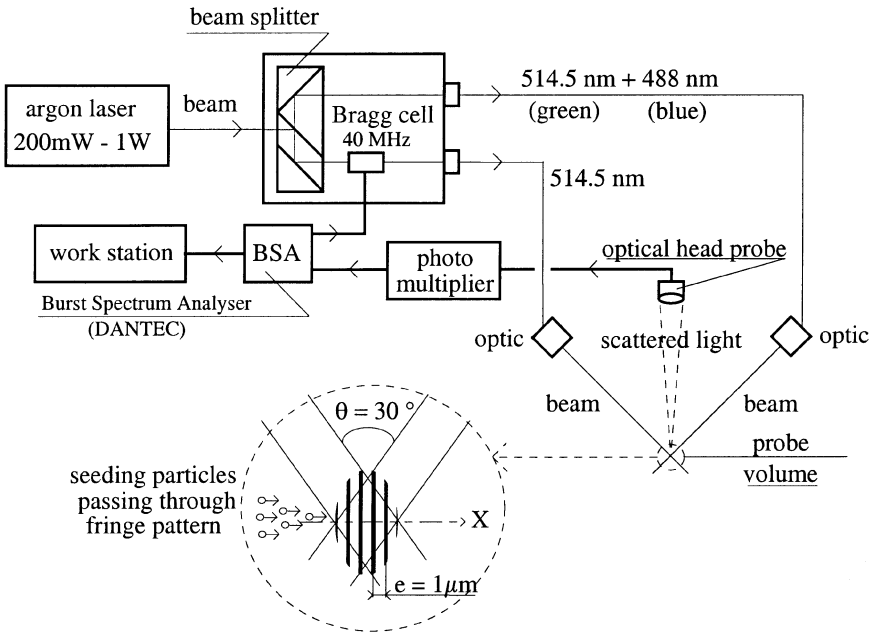

Fig. 3. Layout of laser Doppler anemometer. The analysed volume is located at the crossing point of the two beams. The optical probe head collects the back scattered light emitted by each particle crossing the ellipsoidal analysed volume. Then the optical signal is received by the photomuliplier and treated.

To estimate the velocity from a Doppler signal, a Burst Spectrum Analyser (BSA) performs a spectrum analysis (the spectrum analysis consists of the calculation of the power spectrum of the signal through the use of Fourier techniques).

In order to provide seeding particles in the flow, a fog generator based on water condensation (aerosol) is used. The seeding particles should be small enough to follow the gas flow but large enough to significantly scatter the light. In this specific problem, the velocity of the gas flow is small so the quantity of seeding needed is very small, and must be provided at a very low speed (≈10 cm/s) to avoid perturbation of the velocity measurements.

4.3 Results

Figure 4 shows the current-voltage (I–V_{HT}) characteristic of the point-to-grid obtained with and without seeding

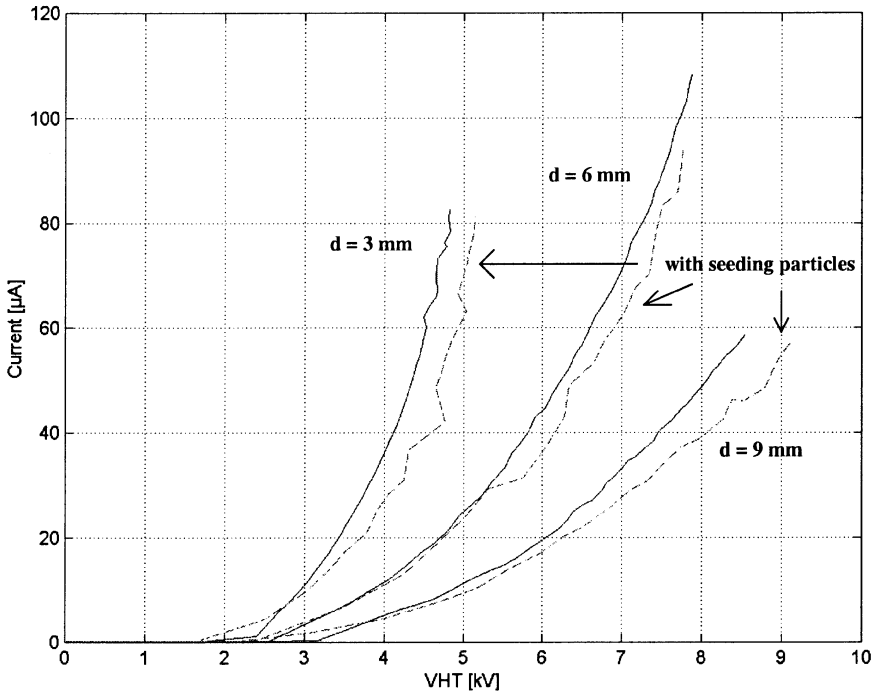

Fig. 4. Current-voltage (I–V_{HT}) characteristics of point-to-plane air gap with and without seeding particles.

particles (water condensation) and at three different gap lengths ($d \approx 3$, 6, 9 mm). With the presence of seeding particle, the corona onset voltage (threshold voltage) and the slope of (I–V_{HT}) characteristic decrease. At constant applied voltage (V_{HT}), the current I decreases with the presence of the seeding particles.

Figure 5 displays the on-axis axial gas velocity in a needle-to-grid corona discharge with different geometric configurations (gap length $d \approx 3$, 6, 9 mm) and electric configurations ($25 \leq I \leq 80$ μA). The errors associated with the measured velocity are principally due to the electric variations of the discharge and are roughly estimated to be ± 0.5 m s^{-1}. The measured velocities between the electrodes have low values ($V_{\mathrm{g}} < 9$ m/s) and the gross feature observed is that the velocity increases with increasing current I, which is in accordance with (Eq. (9)). Whatever the geometric and electric configurations, the measured velocity decreases abruptly near the point and decreases very slowly toward the grid. These behaviours are not predicted by the model which suppose the current density constant along the gap even if the electric field is known as nonuniform. Close to the point, the measuring volume of the LDA technique partially covers the ionisation region and the drift region, the cause of the low velocities measured near the point ($2.5 < V_{\mathrm{g}}$ [m/s] < 5) is not clear, but could be due to the presence of the ring vortex gas flow generated by the positive ions [11,12]. The perturbation of the gas flow near the grid can be attributed to the grid which is not perfectly transparent, and to the presence of water droplets on the grid due to the seeding. Because of the lack of experimental data between the electrodes (data at $x = 0$ and $x = d$ are disregarded), the model cannot be quantitatively validated, and further investigations are needed.

5 Electric wind profiles

In this section, the radial distributions of the axial velocity inside a needle-to-grid system are measured and discussed.

5.1 Experimental set-up

The radial distribution of the electric wind between the electrodes of a point-to-grid system is also obtained using the Laser Doppler Anemometry. The experimental set-up is identical to that already presented in the previous section (Fig. 6). The point-to-grid system has been used with the same electric and geometric configurations [35].

5.2 Results

Figure 7 displays representative evolutions of the gas velocity profile between the electrodes. Whatever the electric and geometric configuration, the gas flow follows a similar profile, and, as already observed (Fig. 5), the flow has low velocities near the point. The velocity increases with the increasing distance from the point x. Near the grid, the velocity profile steepens; this behaviour is due to turbulence created by the wires of the grid which is not perfectly transparent.

Figure 8 shows a comparison between the measured velocity profile and a $\cos^5\theta$ distribution (Warburg law)

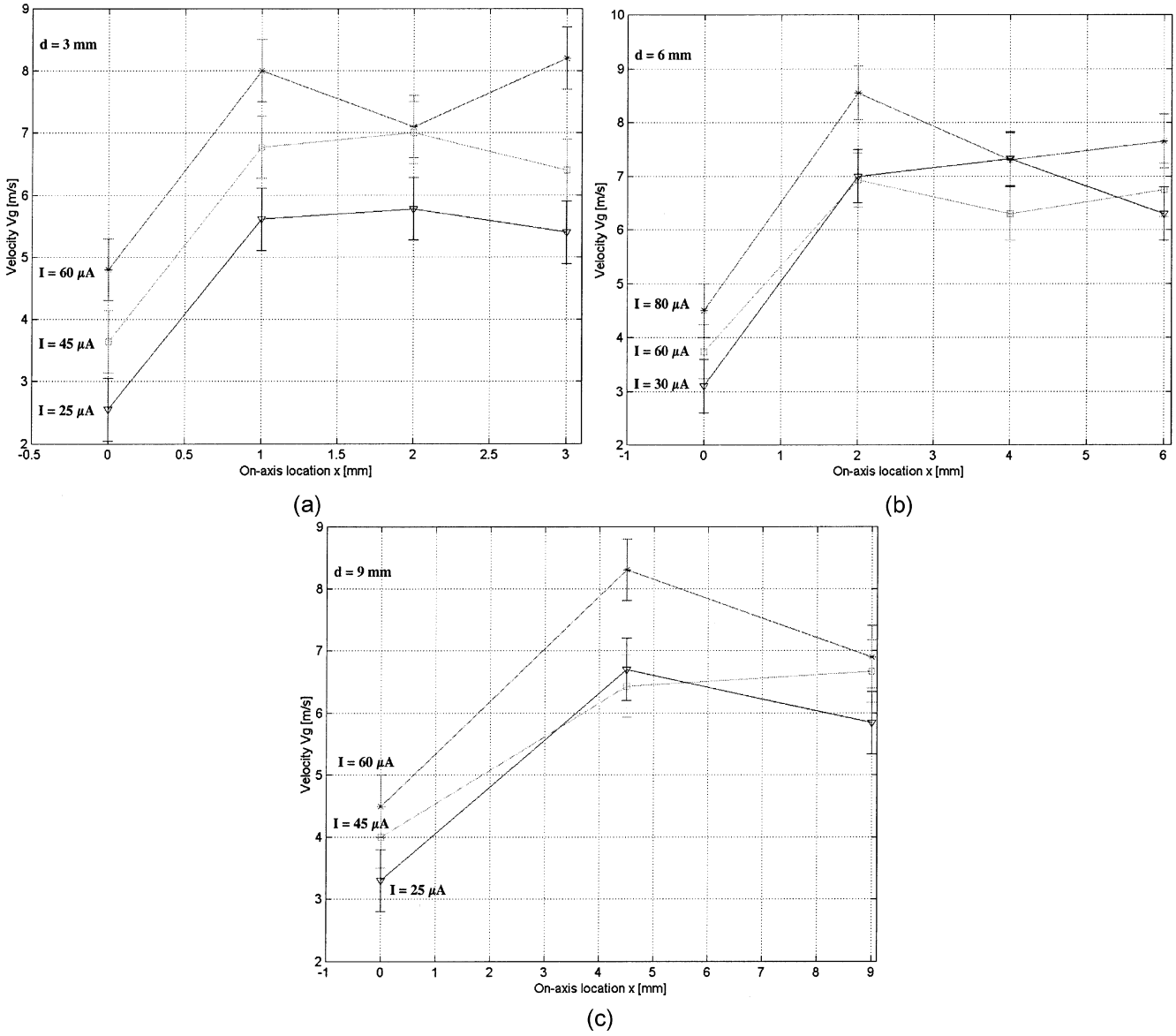

Fig. 5. Axial velocity *versus* the on-axis location x for different geometric configurations (gap length $d \approx 3$, 6, 9 mm) and electric configurations $25 \leq I \leq 80$ μA.

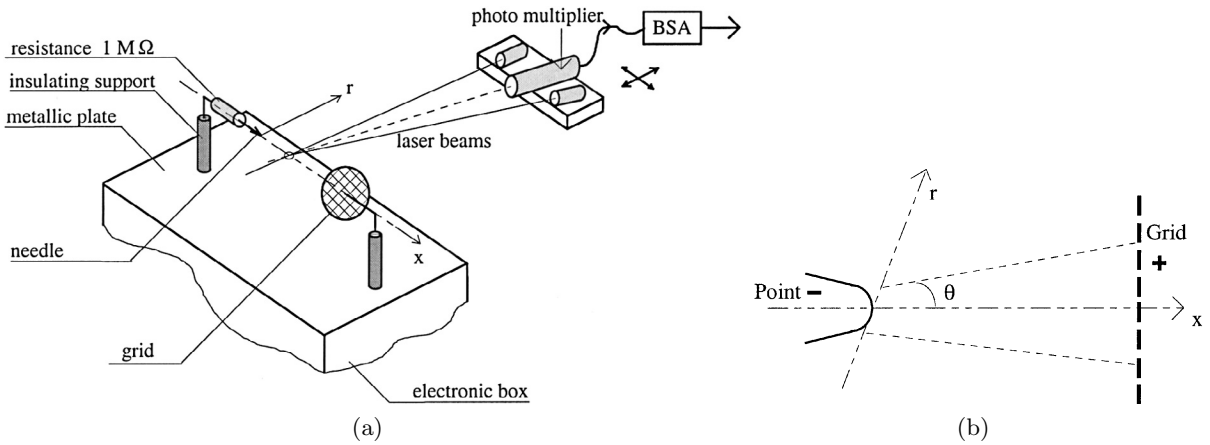

Fig. 6. Schematic representation of the experimental set-up used to measure the velocity profiles with laser Doppler anemometry. Point-to-grid system with r the radial and x the horizontal coordinates.

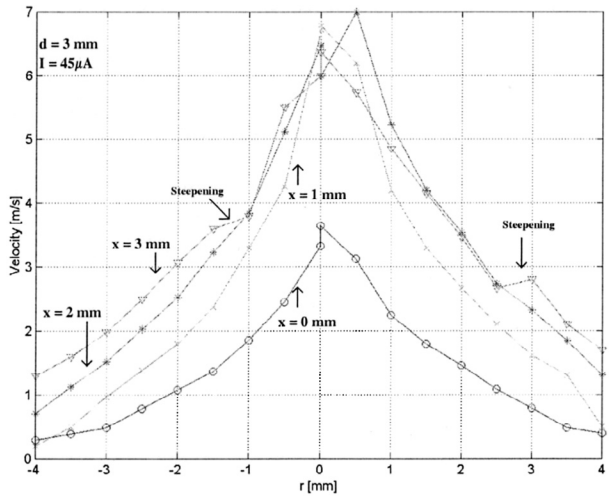

(a)

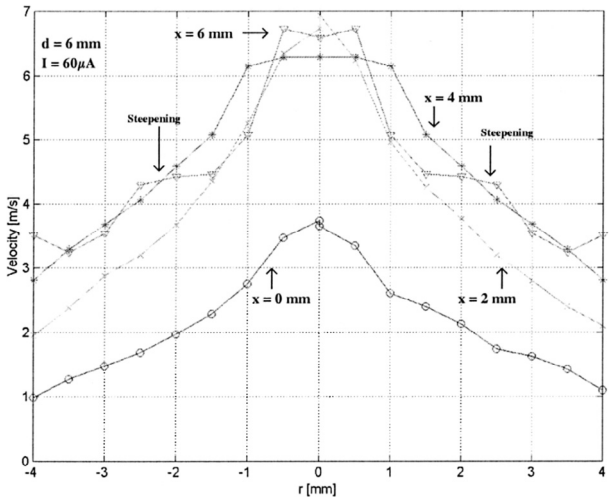

(b)

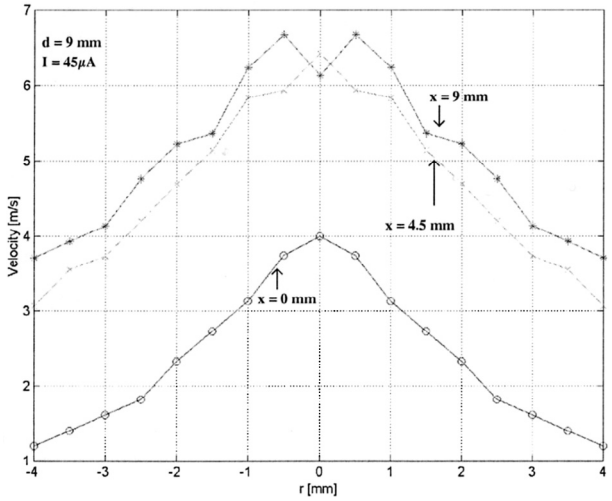

(c)

Fig. 7. Representative velocity profiles *versus* the radial distance r for different geometric configurations (gap length $d \approx 3$, 6, 9 mm) and electric configurations ($I \approx 45$, 60 μA) at different locations ($0 \leq x \leq d$).

where θ is the cone-angle of the discharge (Fig. 6) which is used to model the planar current-density distribution of a negative point-to-plane discharge. The measured velocity profile and the $\cos^5 \theta$ distribution are in close agreement for $r \geq 1$ mm and significant differences can be observed near the discharge axis. These discrepancies could be attributed to the seeding particles. Indeed, the presence of the seeding particle (fog with water particles) introduces humidity between the electrodes which perturbs the electric behaviour of the corona discharge (Fig. 4). Some authors have investigated the effect of humidity on the current density profiles [36–38]. The experimental results reveal that the humidity affects the current density profiles and mainly the central characteristics of the profiles [36]. Further investigations are needed to confirm this last hypothesis.

6 Summary and conclusions

This paper gives the one-dimensional model of the neutral particle velocity associated with a gas flow inside a negative point-to-plane corona discharge in air. The LDA technique measuring on-axis velocity and gas velocity profile between electrodes. The experimental measurements seem to roughly corroborate the predicted behaviours concerning both the current dependence and the location dependence. The lack of agreement observed between the experimental results and the predictions could be attributed to two phenomena:

- mechanisms in the ionisation region (ring vortex flow) which influence the gas movement are not taken into account in the proposed model;
- the seeding particles necessary for the gas velocity measurements with the LDA technique perturb the behaviour of the corona discharges.

Further work is recommended in several areas:

(i) improvement of the model by considering a more accurate current density distribution in the air gap;

(ii) development of the proposed model for the on-axis velocity in which ring vortex flow near the point is considered, and measurement of the transverse velocity to evaluate the vorticity;

(iii) study of the relative affect of the seeding particle on the behaviour of the corona discharges (humidity, entrainment process).

The authors would like to thank Guy Tournois and Philippe Rouquier for the technical advice and interesting discussions. We further wish to thank A. Goldman and M. Goldman for their comments and suggestions on an earlier version of this manuscript.

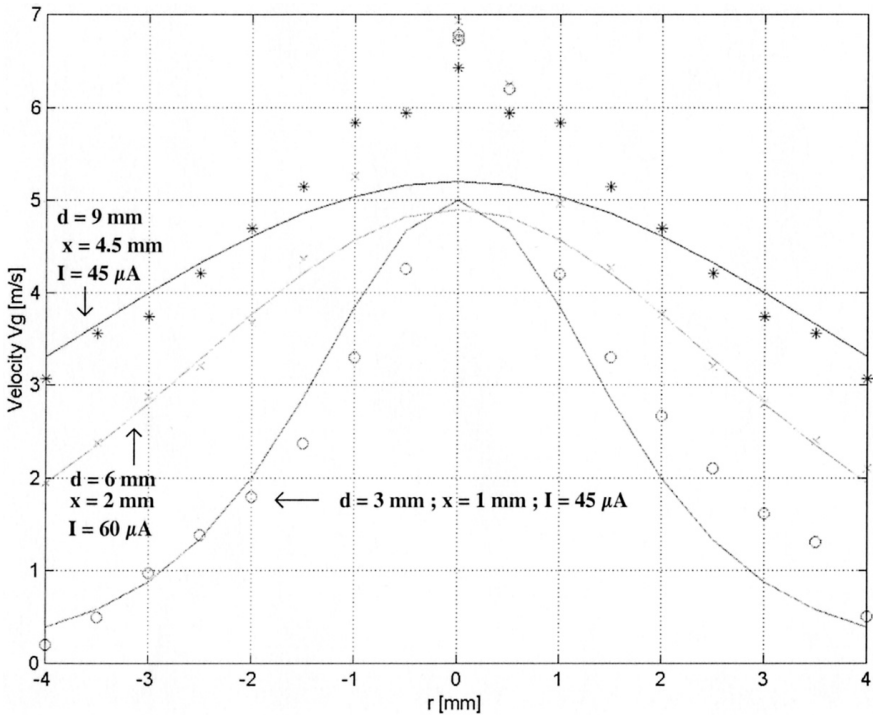

Fig. 8. Representative velocity profiles *versus* the radial distance r for different geometric configurations (gap length $d \approx 3$, 6, 9 mm) and electric configurations ($I \approx 45$, 60 μA) together with a "$\cos^5 \theta$" distribution (Warburg law) where θ is the cone-angle of the discharge (Fig. 6).

References

1. L.B. Loeb, *Electrical coronas* (University of California Press, 1965)
2. E. Nasser, *Fundamentals of Gaseous ionisation and plasmas electronics* (Wiley, New York, 1971), Vol. 1
3. W.L. Lama, C.F. Gallo, J. Appl. Phys. **45**, 103 (1974)
4. M. Goldman, A. Goldman, *Gaseous electronics* (Academic Press, New York, 1978), Vol. 1
5. E.E. Kunhardt, L.H. Luessen, *Electrical breakdown and discharges in Gases* (Plenum Press, New York, 1982)
6. Y.P. Raiser, *Gas discharge physics* (Springer-Verlag, Berlin Heidelberg, 1991)
7. J.E. Jones, J. Phys. D: Appl. Phys. **32**, 1243 (1999)
8. J. Paillol, P. Espel, T. Reess, A. Gibert, P. Domens, J. Appl. Phys. **91**, 5614 (2002)
9. M. Robinson, Trans. Am. Inst. Elect. Engin. **80**, 143 (1961)
10. R.S. Sigmond, Rev. Int. Hautes Tempér. Réfract., Fr. **25**, 201 (1989)
11. R.S. Sigmond, A. Goldman, M. Goldman, Ring vortex gas flow in negative point coronas, *Proc. 10th Int. Conf. On Gas Disch. And their Appl., Swansea, UK, 1992*, pp. 330–333
12. R.S. Sigmond, I.H. Lågstad, Plasma Phys. Rep. **2**, 221 (1993)
13. Y.S. Akishev, I.V. Kochetov, A.P. Napartovich, N.I. Trushkin, Plasma Phys. Rep. **21**, 179 (1995)
14. A.P. Napartovich, Y.S. Akishev, A.A. Deryugin, I.V. Kochetov, M.V. Pan'kin, N.I. Trushkin, J. Phys. D: Appl. Phys. **30** 2726 (1997)
15. Y.S. Akishev, M.E. Grushin, I.V. Kochetov, A.P. Napartovich, N.I. Trushkin, Plasma Phys. Rep. **25**, 922 (1999)
16. L.C. Thanh, Electron. Lett. **15**, 57 (1979)
17. P. Ballereau, Étude du vent électrique. Contribution à l'étude et à la réalisation d'un détecteur de pollution, Ph.D. Thesis, Université Paris-Sud centre Orsay, France, 1980
18. H. Bondar, F. Bastien, J. Phys. D: Appl. Phys. **19**, 1657 (1986)
19. Ph. Béquin, V. Montembault, Ph. Herzog, Eur. Phys. J. AP **15**, 57 (2001)
20. B.L. Owsenek, J. Seyed-Ygoobi, R.H. Page, ASME J. Heat Transfer **117**, 309 (1995)
21. J. Batina, F. Noël, S. Lachaud, R. Peyrous, J.F. Loiseau, J. Phys. D: Appl. Phys. **34**, 1510 (2001)
22. P. Bayle, M. Bayle, G. Forn, J. Phys. D: Appl. Phys. **18**, 2395 (1985)
23. P. Bayle, M. Bayle, G. Forn, J. Phys. D: Appl. Phys. **18**, 2417 (1985)
24. P. Bayle, P. Vacquie, M. Bayle, Phys. Rev. A **34**, 360 (1986)
25. P. Bayle, P. Vacquie, M. Bayle, Phys. Rev. A **34**, 372 (1986)
26. R. Robson, B. Paranjape, Phys. Rev. A **45**, 8972 (1992)
27. O. Eichwald, Modélisation de la dynamique des neutres dans une décharge transitoire : application aux microsystèmes électroniques et aux dispositifs de dépollution, Ph.D.

Thesis, Université Paul Sabatier de Toulouse, Toulouse, France, 1997
28. R.S. Sigmond, J. Appl. Phys. **53**, 891 (1982)
29. R.S. Sigmond, J. Electrostat. **18**, 249 (1986)
30. M.R. Madani, T.A. Miller, IEEE Trans. Ind. Appl. **47**, 907 (1998)
31. E. Francke, J. Amouroux, Plasma Chem. Plasma Process. **17**, 433 (1997)
32. E. Francke, S. Robert, J. Amouroux, High Temp. Mater. Process. **4**, 139 (2000)
33. V. Montembault, Étude des sources acoustiques associées aux décharges corona négatives, Ph.D. Thesis, Université du Maine, Le Mans, France, 1997
34. J.C. Valière, Ph. Herzog, V. Valeau, G. Tournois, J. Sound Vibrat. **229**, 607 (2000)
35. K. Castor, Caractérisation des sources acoustiques associées aux décharges couronnes négatives, Ph.D. Thesis, Université du Maine, Le Mans, France, 2001
36. A. Goldman, M. Goldman, J.E. Jones, M. Yumoto, Current distributions on the plane for point-plane negative coronas in air, nitrogen and oxygen, *Proc. 9th Int. Conf. On Gas Disch. And their Appl., Venezia, Italy, 1988*, pp. 197–200
37. A. Robledo-Martinez, J. Electrostat. **29**, 101 (1992)
38. M. Boutlendj, N.L. Allen, IEEE Trans. Electr. Ins. **28**, 86 (1993)